

# Chemical abundances in cool metal rich disk dwarf stars<sup>\*</sup>

P. Thorén<sup>1</sup> and S. Feltzing<sup>2</sup>

<sup>1</sup> Uppsala Astronomical Observatory, Box 515, 751 20 Uppsala, Sweden

<sup>2</sup> Lund Observatory, Box 43, 221 00 Lund, Sweden

Received 5 June 2000 / Accepted 17 September 2000

**Abstract.** The present study of spectra of twelve metal-rich cool dwarf stars, carefully selected in order to cover a range of temperatures ( $\sim 4400 - 6000$  K), is a follow up on Feltzing & Gustafsson (1998) with the aim to understand the apparent over-ionization and anomalous elemental abundances found by them for the K dwarf stars in their sample.

Our method of analysis employs synthetic spectra of the full spectrum both to constrain the continuum level and to derive abundances. It is shown that by using this method and imposing a strict excitation equilibrium (possible to do because of the care in selection of observed Fe I lines) we are able to show that metal-rich K dwarf stars do not show anomalous stellar abundances, as indicated in Feltzing & Gustafsson (1998), and can, with reasonable efforts, be analyzed in order to increase the number of metal-rich stars with useful chemical abundances.

With abundance analysis by means of spectrum synthesis and assuming Local Thermodynamic Equilibrium (LTE) the abundances of Na, Si, Ca, Sc, Ti, V, Cr, Fe, Co, Ni, and Nd have been derived. Also ionization balance is satisfied for Fe and Cr after correcting the stellar effective temperatures such that both ionization and excitation equilibrium were satisfied.

In addition, spectra from five cool dwarf stars of the Feltzing & Gustafsson (1998) sample have been analyzed with the methods used in this work. They show essentially the same abundance patterns as the new stars in this sample.

**Key words:** stars: late-type – stars: abundances

## 1. Introduction

The atmospheres of dwarf stars retain, except for a small number of elements, the chemical composition of the gas they were formed out of. This makes them ideal as tracers of the galactic chemical evolution. Combining chemical and kinematical data is a powerful method in studies of the galactic chemical evolution. The last decade have seen several studies of stellar abundances of large numbers of dwarf stars with known kinematics and derived ages, eg. Edvardsson et al. (1993) (hereafter

EAGLNT93), Feltzing & Gustafsson (1998) (FG98), Fuhrmann (1998) and Chen et al. (2000). These studies have mainly been concerned with the warmer F and G dwarf stars and the general trends of the different elements are now well established and their gross features can be reproduced, for most elements, by models of galactic chemical evolution, eg. Samland (1998) and Timmes et al. (1995). Well defined abundance trends for stars more metal rich than the Sun can also provide vital clues to the production sites of several elements (see Samland, 1998).

The evolution above  $[\text{Fe}/\text{H}] \sim 0.1$  dex is still, however, fairly poorly sampled and several elements show large scatter. One reason for this is the relative rarity of the most metal-rich stars. FG98 studied a sample of 47 F, G and K dwarf stars with metallicities above solar. In general they confirmed the trends found in EAGLNT93, now also confirmed in Chen et al. (2000). However, for the cool K dwarf stars in their sample FG98 found both an apparent over-ionization as well as odd abundances for several elements. Thorén (2000) has shown that the odd Ca abundances were not, as originally thought, due to NLTE effects (see also Drake 1991), but wrongly calculated damping parameters. The other effects, though, remain to be explained.

Sect. 2 describes the observations. Sect. 3 reports on the data reduction and analysis. In Sect. 4 the stellar abundances are presented. This is followed by a discussion in Sect. 5 and conclusion in Sect. 6.

## 2. Observations

### 2.1. Selection of objects

In order to, as efficiently as possible, study the behaviour of Ca and departures from ionizational equilibrium in metal-rich dwarf stars we have selected stars with a wide range of effective temperatures ( $\sim 4400 - 6000$  K).

In our selection of stars we used stellar parameters derived from Strömgren photometry using the calibration in Olsen (1984). The stars are not distant and interstellar reddening is therefore expected to be negligible and was not taken into account. The data for the ten stars selected in this way are presented in the first part of Table 1. Three of these stars, HD 32147, HD 61606A and HD 69830, were previously studied by FG98. Two other dwarf stars, HD 4307 (HR 203) and HD 20807 (HR 1010), studied in EAGLNT93, were chosen to provide a consistency

Send offprint requests to: Patrik Thorén

<sup>\*</sup> Based on observations made at ESO, La Silla

**Table 1.** Stellar model parameters, both as first derived from photometry and as derived from the stellar spectra themselves after iteration (see Sect. 3.6) and used in the final abundance analysis. Resulting abundances are presented in Table 5. G=typical Gaussian profile FWHM convolved with models to fit observed spectra.  $\log g_\pi$  = surface gravities calculated from Hipparcos parallaxes, see Sect. 3.6. The two stars in Sect. 2 of the table are the hot metal poor dwarfs in common with EAGLNT93. The parameters showed are the same as EAGLNT93 used in their analysis. The last five stars are parameters of FG98 stars - the 2.7m McDonald spectra from that sample have been analysed with the methods described in this work.

ID	Photometry			Spectroscopy			$\xi$	G	$\log g_\pi$	
	$T_{\text{eff}}$	$\log g$	[Me/H]	$T_{\text{eff}}$	$\log g$	[Me/H]				
HD 12235	5971	4.18	0.15	5971	4.18	0.15	1.1	7.5	4.07	
HD 21197	4457	4.59	0.13	4657	4.59	0.27	0.6	5.0	4.55	
HD 23261	5132	4.44	0.06	5132	4.64	0.06	0.9	4.5		
HD 30501	5174	4.54	0.13	5174	4.54	0.13	1.0	5.0	4.47	
HD 31392	5390	4.29	0.06	5390	4.59	0.06	0.7	5.0	4.40	
HD 32147	4625	4.57	0.17	4825	4.57	0.29	0.7	4.5	4.48	
HD 42182	4917	4.54	0.25	5117	4.54	0.10	0.9	5.0	4.46	
HD 61606A	4833	4.55	0.06	4833	4.55	0.06	1.0	5.0	4.46	
HD 69830	5484	4.34	0.10	5484	4.34	0.10	1.2	5.3	4.45	
HD 213042	4560	4.58	0.06	4760	4.58	0.19	1.0	4.5	4.51	
HD 4307	HR 203			5809	4.06	-0.38	1.7	5.5	3.88	
HD 20807	HR 1010			5889	4.41	-0.26	1.3	5.5	4.36	
HD 77338		5290	4.50	0.45	5290	4.60	0.22	1.0	4.5	4.37
HD 87007		5300	4.50	0.43	5300	4.40	0.27	1.0	4.5	4.41
HD 103932		4510	4.58	0.21	4510	4.28	0.16	1.0	4.0	4.49
HD 131977		4585	4.58	0.18	4585	4.58	0.04	1.0	3.5	4.50
HD 136834		4765	4.56	0.23	4765	4.17	0.19	1.0	5.0	4.39

check on both reductions as well as the subsequent abundance analysis. The data for these two stars are presented in the second part of Table 1.

HD 26441 was originally selected as a program star, however it soon became clear that this is a double lined binary star. This was not known at the time of selection, but has later been confirmed by Martin & Mignard (1998). Attempts have been made to determine the abundances for this double star, but the uncertainties proved to be too large. However, the spectra show that the masses must be rather similar. Assuming a similar metallicity ( $[\text{Fe}/\text{H}]=0.15$ ) of the two components the difference in masses (which give the temperature and radius) suggest one component of solar mass and one of slightly lower mass. This is consistent with the results by Martin & Mignard (1998), who find  $M_1 = 1.036 \pm 0.209 M_\odot$  and  $M_2 = 0.824 \pm 0.168 M_\odot$ .

Finally, we also include a re-analysis of stellar spectra for five dwarf stars, originally taken for FG98. These are presented in the third part of Table 1.

## 2.2. Selection of wavelength regions

The Long Camera on the CES only allows observation of one short wavelength interval at a time, typically a few times  $10 \text{ \AA}$ . This means that we had to make a careful selection of wavelength regions. Seven wavelength regions were selected such that a maximum number of unblended strong and weak Ca lines were observed.

The choice of wavelength regions was made so as to maximize the numbers of useful (for abundance determination) lines from elements other than Ca. In particular we wanted to cover a large range in excitation potential for Fe I lines (this later proved vital for our analysis) as well as Fe II, Ni I, Cr I and Cr II.

We were furthermore guided in our selection by the solar line table by Moore et al. (1996) and the solar atlas by Kurucz et al. (1984). Our final seven wavelength regions are centered at 5248, 5880, 6105, 6162, 6445, 6798, and 8520  $\text{\AA}$ . For spectral coverage of single stars, see Table 2. Note, for the five re-analysed stars, that these spectral regions were not analysed in FG98.

## 2.3. Instrumental setup and observations

The spectra were obtained with the ESO CAT-CES November 19 - December 1 1995. The Long Camera and CCD 38 were used, with a nominal spectral resolution of 70,000-100,000, depending on wavelength region. The true resolution is slightly lower in the blue due to bleeding in the CCD. Typical S/N ratios were between 150 and 200.

Spectra from five stars of the sample of FG98 were also analysed with the methods described in this work. The stars were observed with the 2.7 m telescope at the McDonald Observatory, University of Texas, spring 1994. The results of this subsample should be looked upon with caution since we have not managed to analyse all the lines used in the ESO CAT sample and also since it has been observed with a different instrument.

The description of the McDonald observation run can be found in FG98.

### 3. Reductions and abundance analysis

#### 3.1. Basic reduction steps

The spectra were reduced with the ESO MIDAS Banse et al. (1988) software. First the bias was subtracted from all science and calibration frames. Then the flatfield images were coadded and all science frames divided by these, normalized, flatfields. The stellar and calibration spectra were then extracted from the frames.

Calibration spectra, from a Th-Ar lamp, were obtained for each wavelength setting. The lines in the Th-Ar spectrum were identified using a Th-Ar atlas D’Odorico et al. (1987). Finally the stellar spectra were wavelength calibrated using the LONG context in MIDAS.

A spectrum of a cool dwarf star is rich in lines, which makes the definition of the continuum difficult in many cases. Therefore we did not only use continuum points identified in a solar atlas Kurucz et al. (1984) and the Arcturus Atlas by Griffin (1968) but also calculated synthetic stellar spectra to define the exact continuum.

The final continuum level was decided upon through an iterative process where also the stellar parameters were adjusted to obtain optimal fits to the continuum as well as retaining excitational equilibrium for Fe I.

An example of the quality of our spectra as well as the goodness of the fit of the synthetic spectra to the observed ones is shown in Fig. 1.

#### 3.2. Scattered light

Due to scattered light from an unknown source in the CCD frames, a background varying in both dispersive and cross-dispersive direction had to be removed from them. This background had a similar pattern as the fringing pattern which is normally seen in the red, but with a lower amplitude and sometimes slightly shifted in one or both directions. It was also time-dependent and therefore its effect on the spectra for the fainter stars was very strong. A polynomial function was fitted to the smoothed background with the MIDAS SKYFIT/LONG procedure.

After background subtraction the reduced spectra became considerably cleaner. Without removal of the background the patterns were still visible after division with flatfields, since the flatfields were taken with a short exposure time, not long enough to produce the scattered light background component.

#### 3.3. Stellar parameters

Initial stellar parameters were determined from Strömgren photometry. The colours were taken from the catalogues in Olsen (1993) and Olsen (1994). We used the calibration in Olsen (1984), which is valid for G to K dwarf stars.

**Table 2.** Observed wavelength regions. Asterisks indicate that a star was observed in that wavelength region. The stars are arranged in the same way as in Table 1

Star	5248	5800	6105	6162	6448	6798	8520
HD 12235		*		*	*	*	*
HD 21197	*	*	*	*	*	*	*
HD 23261	*	*	*	*	*	*	*
HD 30501	*	*	*	*	*	*	*
HD 31392	*	*	*	*	*	*	*
HD 32147	*	*	*	*	*	*	*
HD 42182		*		*	*	*	*
HD 61606A	*	*	*	*	*	*	*
HD 69830	*	*	*	*	*	*	*
HD 213042		*		*	*	*	*
The Sun	*	*	*	*	*	*	*
HR 203	*	*	*	*	*	*	*
HR 1010	*	*	*	*	*	*	*
HD 77338	*	*	*		*	*	
HD 87007	*	*	*		*	*	
HD 103932	*	*	*		*	*	
HD 131977	*	*	*		*	*	
HD 136834	*	*	*		*	*	

$$\begin{aligned} \log T_{\text{eff}} &= 0.341(b - y) + 3.869 \\ \log g &= 0.37(b - y) + 4.35 \\ [\text{Me}/\text{H}] &= -5.1dm_1 + 0.07 \end{aligned} \quad (1)$$

for stars with  $b - y > 0.51$  and

$$\begin{aligned} \log T_{\text{eff}} &= 0.469(b - y) - 0.103dm_1 + 0.087dc_1 + 3.947 \\ \log g &= 0.50(b - y) + 4.10dm_1 - 2.56dc_1 + 4.30 \\ [\text{Me}/\text{H}] &= -7.5dm_1 + 1.9dc_1 - 0.04 \end{aligned} \quad (2)$$

for stars with  $b - y < 0.51$ .

The stellar parameters were subsequently changed for some of the stars, see Sect. 3.6 and Table 1.

#### 3.4. Model atmospheres

We used the MARCS code, first described by Gustafsson et al. (1975), to generate the model atmospheres. Since then the program has been further developed in various ways and updated in order to handle the line blanketing of millions of absorption lines more accurately, see EAGLNT93 and Asplund et al. (1997). In particular, these models reproduce the continuous opacity and ionizing radiation field in UV better.

#### 3.5. Atomic line data

Basic line data were taken from the VALD database Piskunov et al. (1995). For Ca we used oscillator strengths from Smith (1981) and, for Ca 6162, from Smith & O’Neill (1975).

For other elements we derived  $\log gf$  values both for the lines in Table A.1 and lines (not used in the abundance analysis)

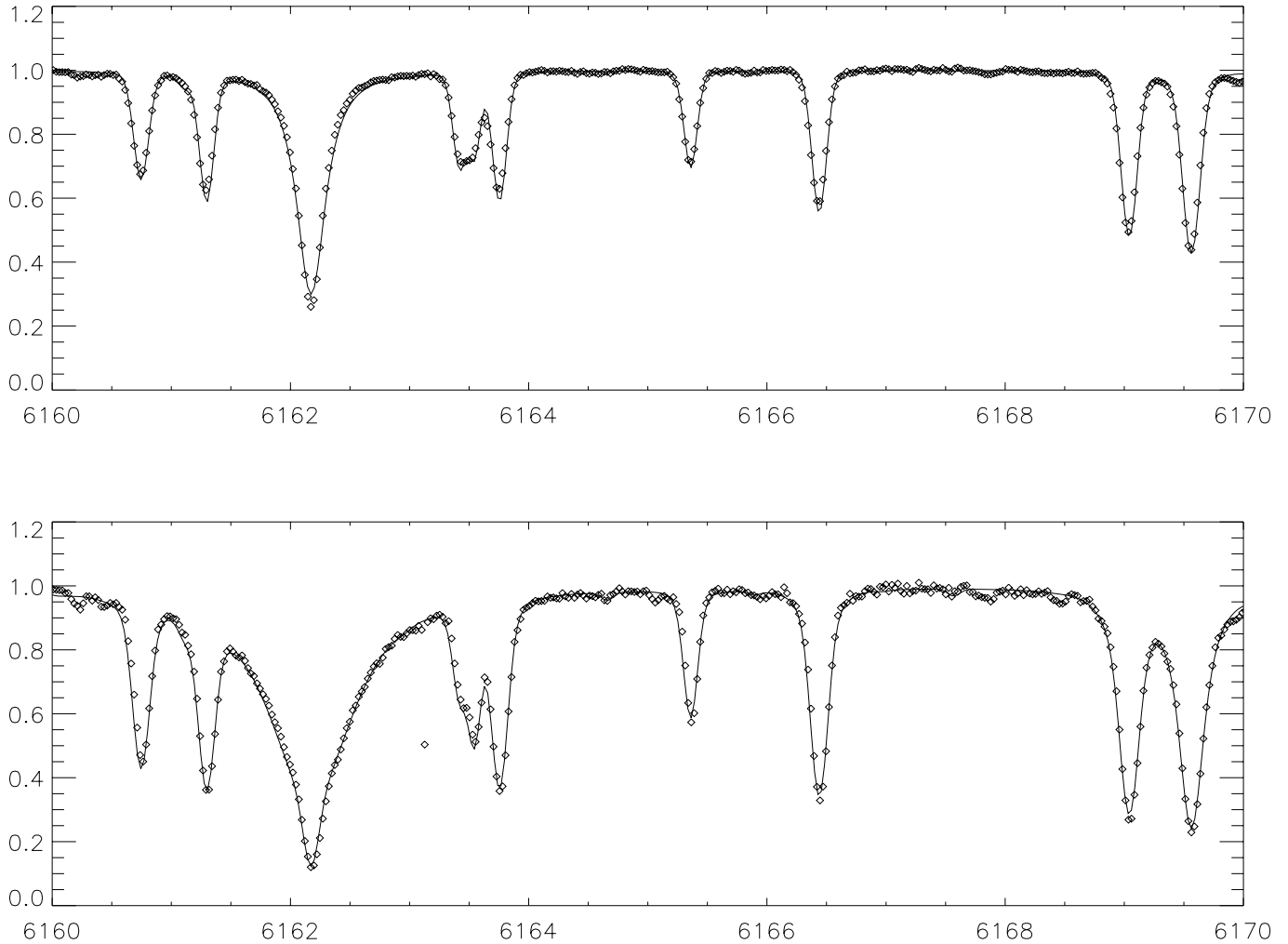


**Fig. 1.** CAT spectrum (diamonds) and synthetic spectrum (solid) of the Sun (upper) and HD 61606A (lower).

in the wings of strong lines. Astrophysical oscillator strengths were derived from the observed solar spectra. For the 6798 Å region no spectrum was achieved for the Sun. A Kurucz solar spectrum was used for that region. The initial values from VALD were usually within the same order of magnitude as the astrophysically fitted values.

Atomic line pressure damping parameters from Anstee & O'Mara (1995), Barklem & O'Mara (1997) and Barklem et al. (1998) were calculated with the Uppsala code SPECTRUM and used for all elements except Ca. These damping parameters give a good fit. The damping calculations are not available for all transitions. For those transitions a  $\delta\Gamma_6$  damping value typical for that element was inserted. These are shown in Table A.1. One of the aims of the project was the comparison of LTE and NLTE analysis for Ca (Thorén, 2000, in preparation). The pressure damping treatment used in SPECTRUM (Anstee & Barklem, 1997 and Barklem, 1998) is not available for MULTI Carlsson (1986) (the code used for the NLTE calculations, see Thorén, 2000, in preparation), therefore pressure damping data for Ca were taken from Smith (1981) and O'Neill & Smith (1980) to achieve maximum consistency with the NLTE analysis.

### 3.6. Abundance determinations

To derive stellar abundances we used standard LTE calculations. The procedure differs in some important ways from that of EAGLNT93 and FG98 and therefore merits a separate discussion. We now briefly describe our iterative process for finding stellar parameters and determine the exact continua in difficult regions:

The instrumental profile was determined by adjusting the width of a Gaussian convolved with the synthetic spectrum generated with SPECTRUM. In the NLTE study (Thorén, 2000, in preparation) the same Gaussian width is used. For some stars the Gaussian width varied with a small amount ( $< 10\%$ ) from region to region. The Gaussian profile simultaneously accounts for the instrumental profile and any effect of stellar rotation and macroturbulence. The Gaussian FWHM width varied between 4.5 and 8.5 km/s (except the spectra from the sample of FG98, some of which had FWHM down to 3.5 km/s). Typical Gaussian widths for each star is given in Table 1.

Observed stellar spectra were compared with synthetic spectra generated with SPECTRUM. To estimate corrections to the stellar parameters derived from the Strömgren photome-

try, equivalent widths were obtained from the fitted synthetic spectra. This was done for the three wavelength regions centred at 6162, 6455, and 6798 Å. These regions are the same as those containing Ca lines in FG98. Using derived abundances for Fe lines and their equivalent widths measured in the synthetic spectra we could constrain effective temperature and microturbulence by imposing excitation balance (effective temperature) and minimizing the spread in derived abundance (microturbulence).

An example, for HD 32147, of corrections with respect to excitation balance is given in Fig. 2. The effective temperature was raised from 4625 K to 4825 K in order to reach excitation balance. In total four of our stars needed temperature adjustments. They were among the coolest stars in the sample and the adopted correction was in all cases +200 K, see Table 1.

In the next step, the other spectral regions were analyzed with synthetic spectra.

The surface gravity was first determined by fitting the pressure broadened Ca I line at 6162 Å. However, when this line was well fitted the quality of the fit of the synthetic spectra in the other regions was not always optimal. For the cool K dwarf stars there are many more lines that are affected by changes in  $\log g$ . We therefore decided to fit the surface gravity by optimizing the fits of strong lines in all wavelength regions. Examples of the fitting are shown in Fig. 3.

The effective temperature and surface gravity parameters were then changed in order to achieve excitation balance in Fe (effective temperature, now using the full spectral coverage) and good fits, in the synthetic spectra, of the wings of strong lines (surface gravity). The choice of surface gravity from synthetic spectral analysis seems to be appropriate also when examining the ion/neutral ratios in Fig. 5 where the signs of overionization is shown to be moderate.

A comparison with surface gravities derived from parallaxes can now be done with the accurate data from Hipparcos (Perryman 1997). With the formula (e.g. Gustafsson et al. 1974)

$$\log \frac{g}{g_{\odot}} = 4 \log \frac{T_{\text{eff}}}{T_{\text{eff}\odot}} + \log \frac{\mathcal{M}}{\mathcal{M}_{\odot}} + 0.4(M_{\text{bol}} - M_{\text{bol}\odot}) \quad (3)$$

we get, with  $M_{\text{bol}\odot} = +4.76$  Mihalas & Binney (1981),  $\log g_{\odot} = 4.44$  and  $T_{\text{eff}\odot} = 5780$

$$\log g = 4 \log T_{\text{eff}} + \log \frac{M}{M_{\odot}} + 0.4V + 0.4B.C. - 2 \log \frac{1}{\pi} - 10.5117 \quad (4)$$

The parallax surface gravities of the dwarves are presented in Table 1. Parallaxes and V-magnitudes were obtained from the Hipparcos catalogue, which contained data for all objects but HD 23261. Masses and bolometric corrections were derived from Table 3–6 in Mihalas & Binney (1981) and the absolute magnitudes derived from the Hipparcos catalogue. Masses for two of the stars, HD 12235 and HD 69830, have been derived by Feltzing et al. (2000) and these agree within 0.02 dex to the masses estimated in this work. The parallax gravities agrees in most cases well with the ones derived by spectroscopy. Note that

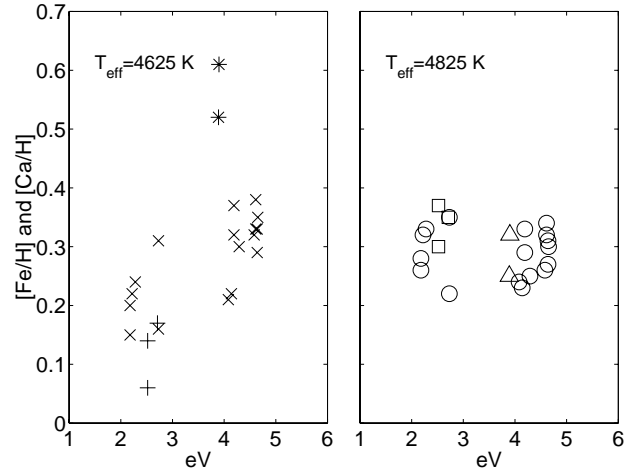


**Fig. 2.** Abundances for different Fe I, Fe II and Ca lines of HD 32147 versus the excitation energy of the lower level.  $\times$ ,  $*$  and  $+$ : Fe I, Fe II and Ca abundances before temperature correction.  $\circ$ ,  $\triangle$  and  $\square$ : Fe I, Fe II and Ca abundances after temperature correction. Note the great Fe II overabundance for the unmodified temperature model.

the largest deviations appears in the re-analysed FG98 sample, which contains less spectra for our abundance analysis.

### 3.7. Error budget from the analysis

#### 3.7.1. NLTE effects in Fe I and Ca I

NLTE abundance errors for low-excitation Fe lines would be important especially for the stars that have required temperature changes to obtain excitation balance in Fe I lines; HD 21197, HD 32147, HD 42182 and HD 213042. These are among the coolest stars, which may raise some suspicion about NLTE effects for low excited Fe I lines for cool metal rich stars. Rentzsch-Holm (1996) and Thevenin & Idiart (1999) calculate Fe NLTE correction for stars with parameters close to the cool dwarf stars in this sample. In both works it seems that NLTE effects decrease and disappear when stellar parameters approach the parameters of our dwarf stars. Therefore we assume that NLTE effects for Fe I can be neglected and that our use of Fe I line excitation balance may safely be used.

NLTE effects in Ca have been explored by Thorén (2000, in preparation). They are shown to be small for cool dwarf stars. For the hotter dwarf stars in this sample LTE Ca abundance values may be slightly too high. However the effects increase with line strength and the lines used in this work never get strong enough to produce significant errors.

#### 3.7.2. Line data

Errors in the atomic line data are restricted to the changes we have made to fit the ESO CAT solar observations, to the broadening parameters calculated with the theories presented in Anstee & O'Mara (1995), Barklem & O'Mara (1997) and Barklem et al. (1998) and to the laboratory measurements presented by Smith (1981). The error in the atomic data from the latter source is re-

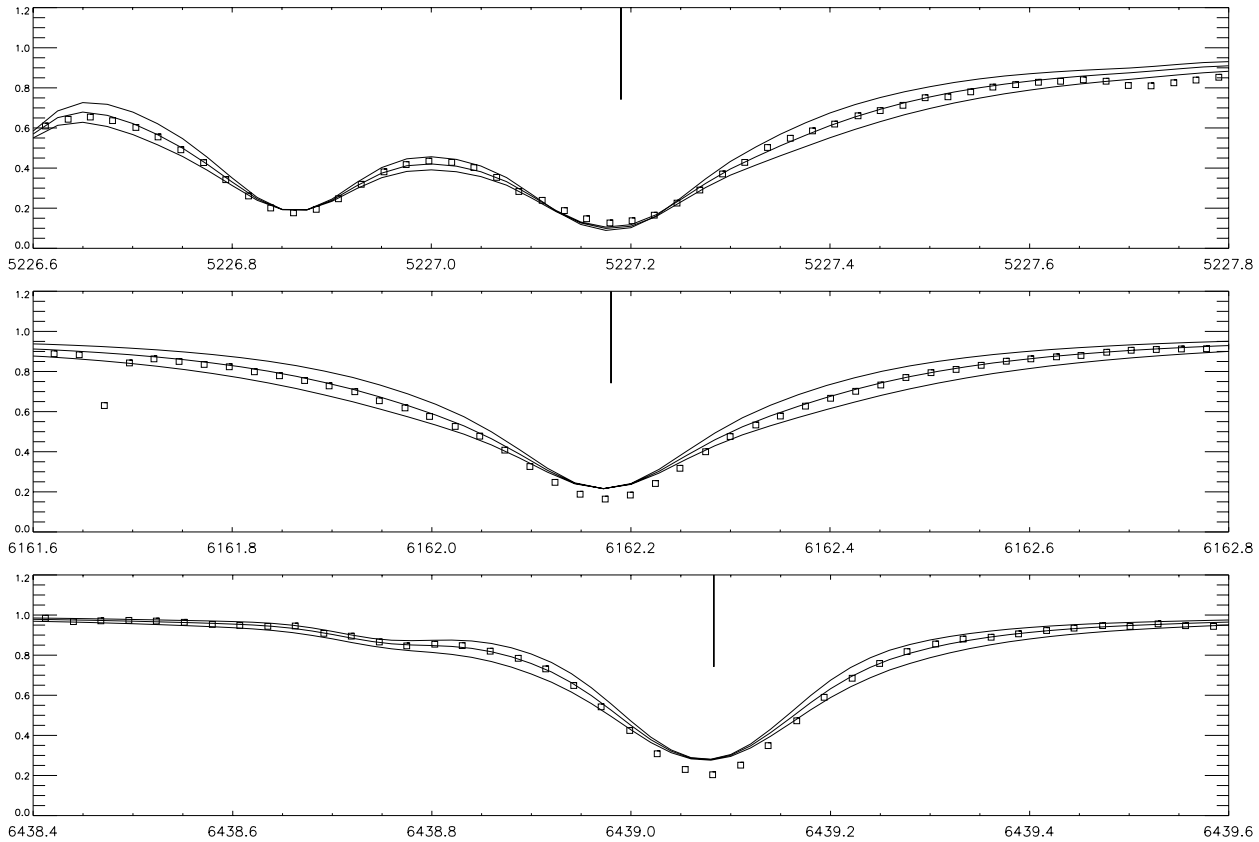


**Fig. 3.** Example of how the surface gravity was fitted, by using several strong lines. Unit on x-axis is Ångström. The normalized flux data (squares) is from the star HD 31392. Three different model gravity spectra are plotted:  $\log g = 4.29, 4.59$  and  $4.89$ . The strong lines displayed are Fe I 5227.19 Å, Ca I 6162.17 Å and Ca I 6139.07 Å. The final surface gravity chosen was  $\log g=4.59$ .

ported to be small ( $<5\%$ ). The theoretically calculated pressure broadening parameters have been tested in Anstee & O'Mara (1995), Barklem & O'Mara (1997) and Barklem et al. (1998) by calculating solar abundances. These abundances are shown to be consistent with meteoritic abundances. In the work presented here erroneous damping parameters would be visible when fitting synthetic spectra. Therefore we conclude that such errors are negligible for our analysis.

The error in astrophysical oscillator strength corresponds to the error in fitting the solar data,  $<0.05$  dex.

### 3.7.3. Continuum fitting

The continuum levels have been drawn with help of synthetic spectra. Thus the errors in these are more dependent on the spectral synthesis than on anything else. Possible errors in the continuum levels have been included in the errors from spectral fitting. These are deemed to be small ( $< 0.1$  dex) and in cases of doubts concerning the continuum level, lines have not been included in the abundance analysis.

### 3.7.4. Background subtraction

The subtracted scattered light background component could possibly introduce an error, if the background model is badly

represented. This would be visible as a continuum difficult to define and such errors are included in the line profile fitting (Sect. 3.7.6).

### 3.7.5. Instrumental profile and macroscopic stellar broadening

The combined line profile broadening by the instrument and any stellar macroscopic broadening were represented by a Gaussian profile that was convolved with the synthetic spectra. This had to be fitted to every new spectral region and star since the resolving power varies with wavelength. The fitting was done by examining the shapes of all lines in an observed spectrum. For most stars and regions the Gaussian profile had a FWHM of  $\sim 5.0$  km/s. If an erroneous profile would be used, the measured abundances would be wrong. The maximum error from misfitted Gaussian profiles is probably  $< 0.05$  dex, considering the large number of lines used to determine the instrumental profile. An inconsistent FWHM value would be visible in form of a systematic shift in the abundances for the wavelength region and star concerned.

### 3.7.6. Synthetic line profile fitting

This error source includes uncertainties in the continuum. In most cases the line fitting uncertainty have been judged to 0.03-

**Table 3.** Stars in common with Edvardsson et al. (1993) (E93).

HR203			HR1010		
Element	[X/H]	E93	Element	[X/H]	E93
Na	-0.36	-0.30	Na	-0.26	-0.22
Si	-0.21	-0.25	Si	-0.20	-0.19
Ca	-0.22	-0.25	Ca	-0.20	-0.20
Ti	-0.19	-0.30	Ti	-0.21	-0.15
Ni	-0.29	-0.29	Ni	-0.27	-0.25
Fe	-0.23	-0.28	Fe	-0.22	-0.23
Fe II	-0.26	-0.31	Fe II	-0.25	-0.33
			Nd II	-0.21	-0.27

0.1 dex. For strong lines it may be larger. However the abundances do not change significantly when the stronger lines are excluded.

### 3.7.7. Errors in derived abundances due to errors in stellar parameters

Because of the method employed in the abundance analysis a straightforward error analysis done by varying the surface gravity and effective temperature used in the model atmosphere is not possible. However, Feltzing (1995) provided such an analysis for two of the K dwarf stars studied here, HD 32147 and HD 61606A, and we may use their derived changes in stellar abundances as a function of model parameters as an estimate of the expected errors in this work. Furthermore FG98 (their Fig. 7) graphically shows how Fe I/Fe II and Cr I/Cr II changes with stellar parameter changes for the two K dwarf stars HD 61606A and HD 103932.

First they find that the two stars, with quite different metallicities, all the same respond with roughly the same changes in abundances because of the changes in model parameters.

In particular Feltzing (1995) find that a change in effective temperature of +200 K would decrease Fe I with -0.03 dex and Fe II with -0.29 dex for HD 32147, thus considerably reducing the apparent overionization. Similar effects were found for HD 61606A and also for Cr. A change in surface gravity of -0.4 dex would change the Fe I abundance with -0.04 dex and the Fe II abundance with -0.21 dex, also almost erasing the overionization. FG98 found no compelling evidence to change the effective temperatures because they did not have a large enough span in excitation energy for the Fe I lines to address excitation equilibrium in the coolest K dwarf stars (they, however, conclude that “we cannot from our analysis exclude that the apparent pattern of overionization... is due to a temperature scale several hundred K too low”). Therefore they kept the effective temperatures and a change of 0.4 dex in the surface gravity was considered too large. The present study show that indeed for HD 32147 the effective temperature should be changed by +200 K.

Further, Feltzing (1995) showed that a change of +200 K meant a change around +0.2 dex for Na, Ca, Si, Ti, and a -200 K change -0.2 dex for the same elements. Si, Cr II, and Fe II would decrease with 0.15 -0.2 dex for an increase of +200 K, and increase with the same amount if the change was -200 K.

The effects on Sc II, Co, and Ni are all smaller than 0.1 dex for changes as large as 200 K.

Since our effective temperatures should have errors smaller or around 100 K we would expect the errors in derived abundances to be smaller than the ones quoted above.

### 3.7.8. Summary of the error analysis

The errors that have been suggested to contribute are (with estimated maximum amplitudes):

NLTE effects	: $\leq 0.05$ dex
Line data	: $\leq 0.07$ dex
Instrumental profile and macroscopic broadening	: $\leq 0.05$ dex
Synthetic line profile fitting	: $\leq 0.10$ dex
Stellar parameters	: $\leq 0.10$ dex

If the errors are uncorrelated, the worst case would produce an error of  $\sim 0.17$  dex. However, this is unlikely, considering the small scatter for most elements seen in Fig. 4.

### 3.8. Comparison with other works

Two stars, HR 203 and HR 1010 were observed for comparison with the results in EAGLNT93. The differences for elements in common are shown in Table 3. The differences are mostly small in comparison with the errors estimated in the two analyses. Notably, there is a difference in Fe (in spite of the large number of neutral Fe lines used in both works) of 0.05 dex for HR 203 and about 0.10 dex for Ti in both stars. Apart from these deviations the agreement is excellent. The differences in Ti go in opposite directions for the two stars, rising doubt about any systematic reason. Due to the stellar parameters (low metallicity and high temperature), any differences in the two analyses probably give very small abundance errors (i.e. easy continuum level definition and spectral line fitting/measuring due to weakness of lines).

Two of the K dwarf stars, HD 32147 and HD 61606A, were also studied by FG98. The difference in abundances are shown in Table 4. There are large differences in the derived abundances for several elements. For HD 32147 the reason is that the stellar parameters derived from the photometry were kept throughout the analysis for these stars in FG98, whereas here we have imposed excitation equilibrium in order to determine the effective temperature. This has resulted, for HD 32147, in a change of +200 K of the effective temperature. In FG98 it was not possible, for the K dwarf stars, to derive effective temperatures from the excitation equilibrium due to a lack of useful Fe I lines at low excitation potential in the observed spectra.

Spectra for five stars of the FG98 sample have been reanalyzed by us with the methods described above (lower part of Table 1). The parameters from FG98 were initially used. Surface gravity was changed for some of the stars. The overlapping spectral regions (only overlapping regions were used, allowing us to use the same set of lines) provided less number of lines than the original set used for our twelve program stars.

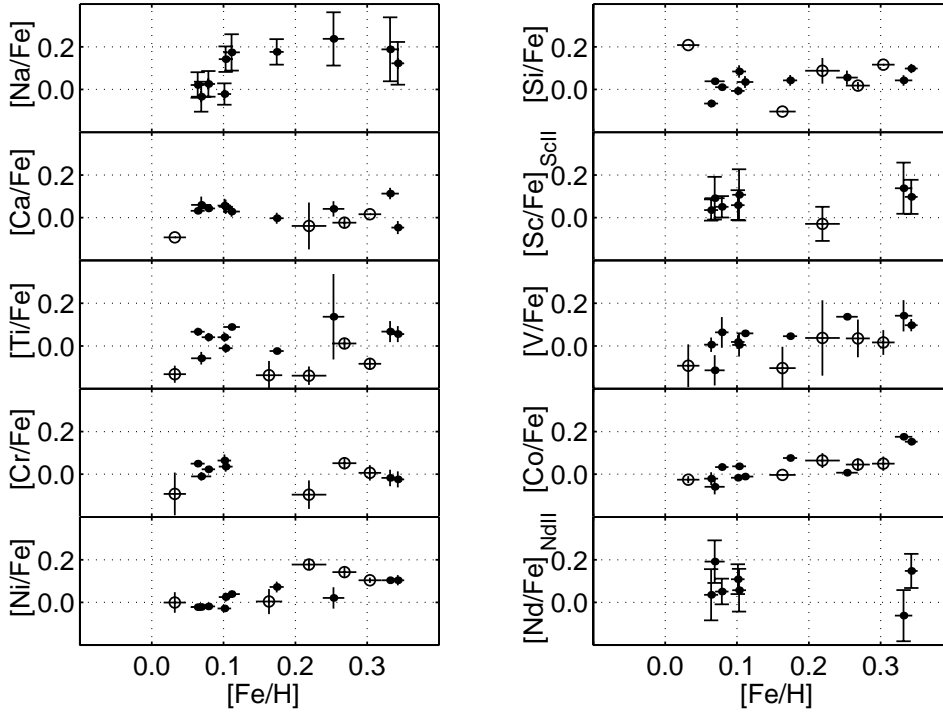


**Fig. 4.** Abundance patterns. Dots: abundances for the ten metal rich stars in the sample of this work. Circles: abundances for the five stars of the FG98 re-analysis sample analysed with the methods described in this work. Error bars: formal error (the error in the mean = line-to-line scatter divided by square root of (number of lines - 1)). For the elements with only one or two lines available the formal error has been replaced with mean uncertainty in the spectral fitting of the lines (error bars with ‘T’ at end).

**Table 4.** Two K dwarfs in common with Feltzing & Gustafsson (1998). Stellar model parameters used in the abundance analysis are shown, as well as the parameters FG98 used. [X/H] give the abundance derived using the stellar models shown (see also Table 1). The columns labeled FG98 present the data originally published in (appendix) Table 1 in FG98, while the F95Recalc column gives the values Feltzing (1995) found when increasing  $T_{\text{eff}}$  in HD 32147 by +200 K as compared to  $T_{\text{eff}}$  given in FG98.

HD 32147			HD 61606A			
$T_{\text{eff}}/\log g$ [Me/H]			$T_{\text{eff}}/\log g$ [Me/H]			
4825 K/4.57/0.29			4833/4.55/0.06			
4625 K/4.57/0.17 (FG98)			4833/4.55/0.11 (FG98)			
	[X/H]	FG98	F95Recalc		[X/H]	FG98
Na	0.46			Na	0.04	-0.25
Si	0.44	0.48	0.31	Si	0.11	0.03
Ca	0.31	0.01	0.18	Ca	0.12	-0.17
Sc II	0.44	0.49	0.45	Sc II	0.16	0.02
Ti	0.40	0.11	0.34	Ti	0.01	-0.09
V	0.44	-0.18	0.06	V	-0.04	-0.46
Cr	0.32	0.10	0.20	Cr	0.06	-0.10
Cr II	0.34	0.78	~0.57	Cr II	0.11	0.24
Fe	0.34	0.22	0.19	Fe	0.07	-0.08
Fe II	0.45	0.61	~0.30	Fe II	0.21	0.09
Co	0.50	0.39	0.40	Co	0.01	-0.11
Ni	0.45	0.57	0.53	Ni	0.05	-0.03
Nd II	0.49			Nd II	0.26	-0.18

The regions are presented in Table 2. We could not justify any change in effective temperature as for the observational sample in this work since the number of available low excited Fe I lines were too low for that decision. It seems however, when studying the abundance patterns and the (lack of) overionization, that

the temperatures of the stellar models are rather well chosen. The resulting abundances are presented in the lower part of Table 5 and the stars are represented in the abundance diagrams by circles. The differences in abundances between FG98 and this work for the five stars are similar to those of HD 32147 and HD 61606A, see Sect. 4 and Table 4.

#### 4. Stellar abundances

We present our final stellar abundances in Table 5 and (excluding the hot, metal poor dwarfs) Fig. 4.

The most notable result for our cool metal-rich dwarf stars is that the two most metal-rich stars (HD 32147 and HD 21197) show almost identical abundance patterns for most of the elements in this study. In particular this is true for V, Co, Sc II, Ti, Si, Cr, and Ni. This is an important finding considering that FG98 found considerable scatter for several of these elements at this metallicity ([Fe/H] = 0.30 dex). The reasons for this are discussed for each element separately below.

The five stars analysed with spectra from the 2.7m McDonald telescope run made by Feltzing in 1994 are in this section referred to as the FG98 re-analysis sample. The abundance patterns of these essentially follow the ones from the stars observed in this work but with larger scatter in many cases. For some elements also a systematic behaviour can be observed. The conclusions of the results are primarily based on the ESO CAT sample.

*Sodium* [Na/Fe] increases with [Fe/H], which is also seen in EAGLNT93 and FG98. The astrophysical oscillator strength ( $\log gf$ ) values used here are essentially the same as in FG98.

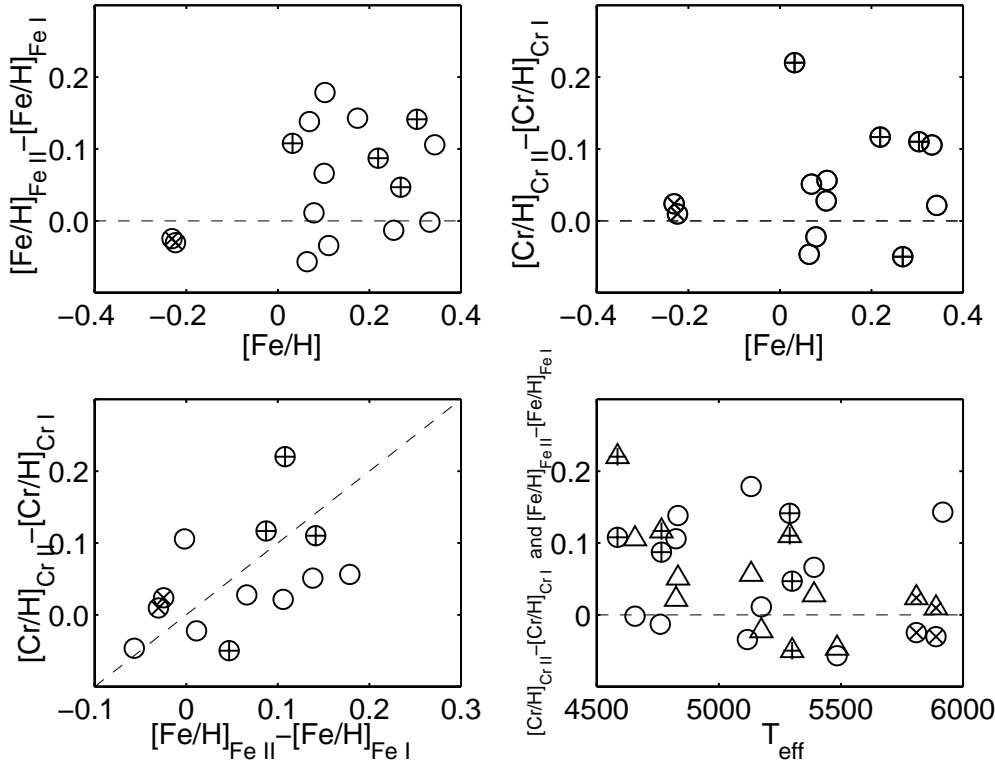


**Fig. 5.** Different ionization patterns. Symbols with pluses represent abundances for stars from the FG98 re-analysis sample, analysed with the methods described in this work. Symbols with  $\times$ s represent abundances for the two hot, metal poor dwarfs. In the last plot Cr is represented by triangles and Fe by circles.

**Table 5.** Stellar abundances. The second section shows the two hot, metal poor dwarfs. The last five stars represent the FG98 re-analysis sample (objects observed 1994 at the 2.7m McDonald telescope, Sect. 2.3).

	Na	Si	Ca	Sc II	Ti	V	Cr I	Cr II	Fe I	Fe II	Co	Ni	Nd II
HD 12235	0.35	0.22	0.17		0.15	0.22			0.17	0.32	0.25	0.25	
HD 21197	0.52	0.37	0.44	0.47	0.40	0.47	0.31	0.42	0.33	0.33	0.51	0.44	0.27
HD 23261	0.24	0.19	0.15	0.21	0.09	0.11	0.14	0.20	0.10	0.28	0.14	0.13	0.16
HD 30501	0.11	0.09	0.12	0.13	0.12	0.14	0.10	0.08	0.08	0.09	0.11	0.06	0.13
HD 31392	0.08	0.09	0.16	0.16	0.14	0.12	0.17	0.19	0.10	0.17	0.08	0.07	0.21
HD 32147	0.46	0.44	0.30	0.44	0.40	0.44	0.32	0.34	0.34	0.45	0.50	0.45	0.49
HD 42182	0.29	0.15	0.14		0.20	0.17			0.11	0.08	0.10	0.15	
HD 61606A	0.03	0.11	0.13	0.16	0.01	-0.05	0.06	0.11	0.07	0.21	0.01	0.05	0.26
HD 69830	0.08	0.00	0.10	0.10	0.13	0.07	0.11	0.07	0.06	0.01	0.04	0.04	0.10
HD 213042	0.49	0.31	0.29		0.39	0.39			0.25	0.24	0.26	0.27	
HR 203	-0.36	-0.21	-0.22	-0.18	-0.19	-0.28	-0.20	-0.18	-0.23	-0.26	-0.19	-0.29	-0.18
HR 1010	-0.26	-0.20	-0.20	-0.26	-0.21	-0.26	-0.25	-0.24	-0.22	-0.25	-0.23	-0.27	-0.21
HD 77338		0.42	0.32		0.22	0.32	0.31	0.42	0.30	0.44	0.35	0.41	
HD 87007		0.29	0.25		0.28	0.30	0.32	0.27	0.27	0.32	0.31	0.41	
HD 103932		0.06			0.03	0.06			0.16		0.16	0.17	
HD 131977		0.24	-0.06		-0.10	-0.06	-0.06	0.16	0.03	0.14	0.01	0.03	
HD 136834		0.31	0.18	0.19	0.08	0.26	0.12	0.24	0.22	0.31	0.28	0.40	

*Silicon* There is a weak overabundance for Si but no increasing trend appears. This result follows that indicated by the metal rich end in EAGLNT93. It does not confirm the overabundance indicated for Si in cool dwarf stars in FG98. 1-3 lines were used in FG98, 13 in this work. The line-to-line scatter in our data is significantly reduced compared with FG98. The error analysis in FG98 (see their Table 3 and also several tables in Feltzing, 1995) indicates that for cool K dwarf stars like HD 32147 an increase in effective temperature of 200 K is followed

by a decrease in derived Si abundance of around 0.15 dex. The  $T_{\text{eff}}$  adjustment in Sect. 3.6 lead to that the K dwarfs follow the same trend for Si as do the G dwarfs.

These new results show that the large scatter seen in [Si/Fe] in FG98 was partly due to a small numbers of (not optimally selected) lines as well as too low effective temperatures for K dwarf stars. We thus conclude that Si varies in lockstep with Fe also for stars more metal-rich than 0.2 dex.

*Calcium* As shown in Thorén (2000), the major reason for the underabundance in Ca for K dwarf in FG98 was due to erroneously calculated line damping parameters for the Ca lines.

Any remaining differences in  $[Ca/Fe]$  between G and K dwarf stars vanishes when the effective temperatures are adjusted to satisfy the excitation balance, Sect. 3.6. The resulting Ca trend and scatter follows what is indicated in EAGLNT93 and in FG98 for the F and G dwarf stars.

*Scandium* One Sc II line was used, four in FG98. They found that Sc II follows Fe, except for the K dwarf stars, where a large underabundance can be seen. This is not the case here, where Sc II follows Fe and the warmer dwarf stars. With only one line no strong conclusions can be drawn, though.

*Titanium* We find  $[Ti/Fe]$  to vary in lock step with Fe also for K dwarf stars. This is in contrast to FG98 where the K dwarf stars were low in Ti as compared to the G dwarf stars. This is understandable. Abundances derived from Ti I lines are sensitive to variations in effective temperature, see Table 3 in FG98 and tables in Feltzing (1995). In fact they found that the effects are larger on K dwarf stars than on G dwarf stars.

The difference of 200 K is enough to bring the Ti I up 0.24 dex, and thus move the K dwarf stars onto solar  $[Ti/Fe]$  and with a small scatter for our main sample. We note however, that the FG98 re-analysis sample shows lower  $[Ti/Fe]$ .

*Vanadium* V is overabundant at high  $[Fe/H]$ . This is opposite to the case seen in FG98 where the K dwarf stars show underabundances. Four lines are used here, two in FG98. Since we here increase the lowest effective temperature by 200 K, Sect. 3.6, we should expect the underabundance seen for K dwarf stars in FG98 to disappear since their error analysis (FG98, Table 3) indicate that an increase of +200 K will result in and V abundance increased by 0.23 dex. Furthermore, care has also to be taken with broadening of the strong lines. As shown in Thorén (2000) erroneous line broadening may be fatal for strong lines. The effect is worst for the coolest, most metal rich stars. This has been checked for V but no effect could be seen when changing the damping scheme of Anstee & Barklem (1997), Barklem (1998) used in SPECTRUM to the values used in FG98. Two lines are used in FG98, one (6452.31 Å) is in common with this work. This line has in FG98 an astrophysical  $\log gf$  value 0.5 dex higher than the one used here. This is probably the reason for the difference in behaviour for V. When the  $\log gf$  value of FG98 is inserted here and the synthetic line fitted, it gives an underabundance of about 0.2 dex.

Taking the five stars of the FG98 re-analysis sample into account the overabundance is somewhat reduced. They do, however, also show an increasing trend with increasing  $[Fe/H]$ .

*Chromium* No sign of Cr under- or overionization is apparent Fig. 5. The data in Fig. 4 follows the trend seen in FG98, except for the K dwarf stars which are underabundant in that work, this

is consistent with the errors analysis presented in FG98 (Table 3) where they show that an increase in effective temperature would result in abundances from Cr I lines would increase by 0.1 dex while those from Cr II would decrease by 0.15 dex, thus reducing the apparent over-ionization drastically.

From our work it is apparent that by imposing excitation equilibrium, see Sect. 3.6, we naturally arrive close to ionization equilibrium as well.

*Iron* A weak Fe overionization (mean  $< 0.1$  dex), with some scatter is seen in Fig. 5. The effect seen for K dwarf stars in FG98 is mostly removed though, and no temperature trend for Fe II can be observed, as seen in Fig. 5.

*Cobalt* An increasing trend with  $[Fe/H]$  and small scatter is apparent for Co. This can be compared to FG98 where an increasing trend is seen for the K dwarfs but not for the other stars. The overabundance here is  $\sim 0.2$  dex for the most metal rich dwarf stars. Eight lines were used in FG98, four lines here. Both their K dwarf stars and the dwarf stars here appear to follow the upper envelope of the slowly increasing  $[Co/Fe]$  trend for the whole sample of FG98. The five stars from the FG98 re-analysis sample moderate the trend somewhat.

*Nickel* FG98 found that Ni varied in lock-step with Fe except the K dwarf stars, which were more abundant in Ni than the G dwarf stars. We show that also the K dwarf stars indeed vary in lock-step with iron also for high metallicities. Taking the five stars from the FG98 sample into account a weak increasing trend is revealed. Part of the decreased  $[Ni/Fe]$  here as compared to FG98 for the K dwarf stars can be attributed to the change in effective temperatures, Sect. 3.6, but not all. Some of the stars in FG98 showed a considerable scatter in  $[Ni/Fe]$  perhaps indicating problems with the analysis of some of the lines used. All of their K dwarf stars, except HD 61606A, show such large scatter, and thus we conclude that part of the high  $[Ni/Fe]$  found for the K dwarf stars in their work was also due to problems with the analysis of some of the Ni lines.

We note, however, that the two most metal-rich stars in our sample are slightly more abundant in Ni than the rest of the sample. The new re-analyzed spectra from the FG98 sample show a weak increasing trend with increasing  $[Fe/H]$ . They additionally show a larger scatter.

*Neodymium* We only use one line for Nd, not the same as the single line used in FG98, and the trend seen in their work is not reproduced here. Rather, Nd seems to follow iron, with a considerable scatter. However, any firm conclusion from this material is impossible.

#### 4.1. Summary and speculations

We show that  $[Si/Fe]$ ,  $[Ca/Fe]$ ,  $[Ti/Fe]$ , and  $[Cr/Fe]$  all varies as  $[Fe/H]$  between 0.00 and 0.35 dex. So does  $[Ni/Fe]$  but with a,

very tentative, upturn for the most metal-rich stars.  $[\text{Co}/\text{Fe}]$  and  $[\text{V}/\text{Fe}]$  increase slowly with  $[\text{Fe}/\text{H}]$ .  $[\text{Na}/\text{Fe}]$  shows a definite increasing trend with  $[\text{Fe}/\text{H}]$ . Taking the results from new observed spectra of the FG98 sample (which has sparser amount of available lines) into account, the  $[\text{Ni}/\text{Fe}]$  increment looks stronger and the  $[\text{Co}/\text{Fe}]$  less convincing.

For Nd the data is uncertain.

We find that the  $\alpha$ -elements such as Si and Ca follow Fe for high metallicities, in contrast to oxygen which is indicated to keep decreasing with increasing  $[\text{Fe}/\text{H}]$  (FG98). This is, perhaps, a first indication of second sources of  $\alpha$ -elements that start to contribute to the galactic chemical evolution on a very long time-scale. This is, of course, a highly speculative suggestion and must await further studies of in particular oxygen to be confirmed or rejected.

## 5. Discussion

For the analysed elements, except V and Co and possibly Ni, the cool dwarf stars show the same behaviour as the warmer ones in the  $[A/A]$  diagrams. A weak dependence with  $[\text{Fe}/\text{H}]$  is sometimes visible but the variations are within the uncertainties. Co and V show a different trend compared to FG98. V here increases with metallicity, while FG98 shows a decrease. The reason may be a different (possibly erroneous)  $\log gf$  value for one of the lines used in FG98. Co is here also weakly increasing while no trend (although a weak, almost insignificant trend is seen for the K dwarf stars) is apparent in FG98. The cool dwarf stars in this work are situated at the upper envelope of the pattern indicated there. Fig. 21 in FG98 shows  $[\text{Co}/\text{Fe}]$  compared with data from other works. A possible increase for increasing  $[\text{Fe}/\text{H}]$  is indeed possible to see when taking the more metal poor stars into account.

No evidence can be found that cool dwarf stars show non-solar abundance ratios, other than Na (and with weak trends for Co, V and possibly Ni). Na is known to increase compared to Fe for increasing metallicity. This behaviour is reproduced here, with a strong trend with increasing metallicity.

Cool metal rich dwarf stars seem to be usable in investigations of Galactic chemical evolution, if synthetic spectral analysis is used, rather than equivalent widths analysis. The radiation fields shown by the modern MARCS code indicate that only weak NLTE effects should be expected also for other elements than Ca.

## 6. Conclusions

The investigation by FG98 left several unexpected results and unanswered questions in particular about elemental abundances in K dwarf stars. Applying new methods, tailored to suite the K dwarf stars, in our abundance analysis we have been able to answer a number of these questions. In particular we find that:

- by imposing excitation balance for Fe I lines we naturally arrive close to LTE ionization balance for Fe and Cr
- stellar abundance results for cool K dwarf stars are more or less the same as for their warmer counter-parts

- we show that the stellar atmosphere models of the coolest stars need temperature corrections as compared to the calibrations presented by Olsen (1984). This may indicate a systematic error in the calibration for the stars with colours  $b - y > 0.51$
- according to the photometric calibration for the metallicity Olsen (1984), HD 42182 is a Super-Metal-Rich (SMR,  $[\text{Me}/\text{H}] > 0.20$ , Taylor, 1996) candidate star. This is not confirmed by our data. Also, HD 21197, which has just above solar metallicity from the photometry is showed to be a SMR star, as well as HD 32147
- the two most metal-rich stars in our sample show extremely similar abundances, which makes it possible to draw strong conclusions on the stellar abundance trends
- $[\text{Si}/\text{Fe}]$ ,  $[\text{Ca}/\text{Fe}]$ ,  $[\text{Ti}/\text{Fe}]$  and  $[\text{Cr}/\text{Fe}]$  all vary as  $[\text{Fe}/\text{H}]$  also for stars more metal-rich than 0.2 dex
- $[\text{Na}/\text{Fe}]$  (and possibly  $[\text{V}/\text{Fe}]$ ,  $[\text{Co}/\text{Fe}]$  and  $[\text{Ni}/\text{Fe}]$ ) increases with increasing  $[\text{Fe}/\text{H}]$ .

*Acknowledgements.* The authors thank Docent Bengt Edvardsson for valuable discussions and comments on the manuscript. The referee is thanked for suggestions that improved the quality of the article. PT was supported by the Swedish Natural Science Research Council, NFR.

## Appendix: atomic line data for the LTE analysis

The following columns appear in Table A.1:  $\chi$  is the excitation energy of the lower level of the line transition.  $\log gf$  is the logarithm of the lines astrophysical oscillator strength times the statistical weight of the lower level of the line transition. For Ca (except the 5867 Å and 6798 Å lines) the  $\log gf$  values were taken from Smith (1981) and Smith & O'Neill (1975).  $\delta\Gamma_6$  represents the value used for pressure line wing damping. Pressure line wing damping was calculated according to Anstee & O'Mara (1995), Barklem & O'Mara (1997) and Barklem et al. (1998) for the lines marked with asterisks. For the lines with a  $\delta\Gamma_6$  value, this was multiplied with the classical Unsöld damping value. The  $\delta\Gamma_6$  values used were 2.50 for all elements except Ca Smith (1981); O'Neill & Smith (1980), Na ( $\delta\Gamma_6=2.00$ ), Si ( $\delta\Gamma_6=1.30$ ) and Fe ( $\delta\Gamma_6=1.40$ ), see EAGLNT93 and references therein.  $\Gamma_{\text{rad}}$  represents the radiative damping constant. The strong lines printed in **boldface** have not been used in abundance analysis, only for estimating the surface gravity, see Sect. 3.6.

## References

- Anstee S.D., O'Mara B.J., 1995, MNRAS 276, 859  
 Asplund M., Gustafsson B., Kiselman D., Eriksson K., 1997, A&A 318, 521  
 Banse K., Ponz D., Ounnas C., Grosbol P., Warmels R., 1988, In: Robinson L.B. (ed.) Instrumentation for Ground-Based Optical Astronomy, Present and Future. The Ninth Santa Cruz Summer Workshop in A&A, July 13–24, 1987, Lick Observatory, Springer-Verlag, New York, NY, p. 431  
 Barklem P.S., O'Mara B.J., 1997, MNRAS 290, 102  
 Barklem P.S., O'Mara B.J., Ross J.E., 1998, MNRAS 296, 1057  
 Carlsson M., 1986, In: Uppsala Astronomical Observatory Report No. 33

**Table A.1.** Atomic line data.

Wavelength (Å)	$\chi$ (eV)	$\log gf$	$\delta\Gamma_6$	$\Gamma_{\text{rad}}$ (s <sup>-1</sup> )
Na				
6154.226	2.102	-1.650	2.00	7.079E+07
6160.747	2.104	-1.320	2.00	7.079E+07
Si				
5873.764	4.930	-3.010	1.30	1.000E+05
6106.608	5.614	-2.230	1.30	1.000E+05
6145.016	5.616	-1.470	1.30	1.000E+05
6131.768	5.082	-3.650	1.30	1.000E+05
6112.928	5.616	-2.250	1.30	1.000E+05
6125.021	5.614	-1.630	1.30	1.000E+05
6433.457	5.964	-1.640	1.30	1.000E+05
6800.596	5.964	-1.740	1.30	1.000E+05
8492.077	5.863	-1.930	1.30	1.000E+05
8501.544	5.871	-1.280	1.30	1.000E+05
8502.219	5.871	-0.910	1.30	1.000E+05
8536.164	6.181	-0.610	1.30	1.000E+05
8556.777	5.871	-0.430	1.30	1.000E+05
Ca				
5260.387	2.521	-1.719	0.91	7.980E+07
5867.562	2.933	-1.641	1.01	2.624E+08
6161.297	2.523	-1.266	1.64	1.879E+07
<b>6162.173</b>	<b>1.899</b>	<b>-0.09</b>	<b>2.48</b>	<b>7.244E+07</b>
6166.439	2.521	-1.142	1.64	1.858E+07
6169.042	2.523	-0.797	1.64	1.977E+07
6169.563	2.526	-0.478	1.64	1.875E+07
<b>6439.075</b>	<b>2.526</b>	<b>0.390</b>	<b>0.65</b>	<b>4.457E+07</b>
6455.598	2.523	-1.290	0.71	4.645E+07
6471.662	2.526	-0.686	0.63	4.416E+07
6798.467	2.709	-2.520	*	1.941E+07
Sc II				
5239.813	1.455	-0.870	2.50	1.330E+08
Ti				
5219.702	0.021	-2.392	*	6.668E+06
5222.674	2.085	-0.621	*	6.026E+07
5224.305	2.134	-0.210	*	6.012E+07
5247.289	2.103	-0.927	*	6.012E+07
5248.383	1.879	-1.418	*	2.312E+08
5265.964	1.887	-0.717	*	2.312E+08
5866.451	1.067	-0.940	*	4.395E+07
6091.171	2.267	-0.473	*	8.492E+07
6092.792	1.887	-1.379	*	1.271E+08
6098.658	3.062	-0.210	*	5.433E+07
6121.001	1.879	-1.522	*	1.230E+08
6126.216	1.067	-1.475	*	9.931E+06
8518.352	1.879	-1.089	*	7.211E+07
V				
5240.862	2.374	0.230	*	6.871E+07
6090.214	1.081	-0.062	*	3.981E+07
6111.645	1.043	-0.915	*	3.899E+07
6452.341	1.195	-1.306	*	3.981E+07

**Table A.1.** (continued)

Wavelength (Å)	$\chi$ (eV)	$\log gf$	$\delta\Gamma_6$	$\Gamma_{\text{rad}}$ (s <sup>-1</sup> )
Cr				
5220.912	3.385	-1.034	2.50	8.110E+07
5224.069	3.410	-1.129	2.50	8.054E+07
5225.814	2.708	-1.519	*	3.622E+08
5228.096	3.369	-0.808	2.50	1.361E+07
5238.964	2.709	-1.505	*	2.541E+08
5240.464	3.668	-0.804	2.50	4.688E+07
5243.364	3.395	-0.667	2.50	8.091E+07
5247.566	0.961	-1.740	*	5.284E+07
5265.157	3.428	-0.519	2.50	8.091E+07
Cr II				
5237.329	4.073	-1.377	2.50	2.553E+08
5246.768	3.714	-2.566	2.50	2.312E+08
5249.437	3.758	-2.789	2.50	2.350E+08
Fe				
<b>5227.151</b>	<b>2.424</b>	<b>-1.352</b>	*	<b>1.449E+08</b>
5837.701	4.294	-2.340	*	4.775E+07
6078.491	4.795	-0.374	*	1.828E+08
6079.009	4.652	-1.020	*	1.932E+08
6082.711	2.223	-3.573	*	7.691E+06
6089.580	4.580	-1.312	1.40	9.268E+07
6093.644	4.607	-1.400	*	1.936E+08
6093.644	4.607	-1.400	1.40	1.936E+08
6094.374	4.652	-1.640	*	1.932E+08
6096.665	3.984	-1.770	*	4.529E+07
6098.245	4.558	-1.840	*	2.618E+08
6105.131	4.548	-2.050	*	1.941E+08
6120.249	0.915	-5.950	*	2.710E+04
6145.420	3.368	-3.600	*	1.175E+08
6151.618	2.176	-3.379	*	1.549E+08
6157.728	4.076	-1.320	*	5.023E+07
6159.378	4.607	-1.970	*	1.919E+08
6165.360	4.143	-1.554	*	8.770E+07
6173.336	2.223	-2.920	*	1.671E+08
6180.204	2.727	-2.686	1.40	1.469E+08
6187.39	2.832	-4.339	*	1.449E+08
6430.846	2.176	-2.006	1.40	1.648E+08
6436.407	4.186	-2.410	1.40	3.041E+07
6469.193	4.835	-0.770	1.40	2.275E+08
6481.870	2.279	-2.984	1.40	1.549E+08
6752.707	4.638	-1.204	1.40	2.301E+08
6756.563	4.294	-2.750	*	7.345E+07
6786.860	4.191	-1.850	1.40	1.986E+08
6794.619	4.955	-2.110	1.40	4.355E+08
6804.001	4.652	-1.546	1.40	1.758E+08
6804.271	4.584	-1.813	1.40	5.236E+07
6806.845	2.727	-3.110	1.40	1.021E+08
6810.263	4.607	-0.986	1.40	2.301E+08
6819.586	4.103	-2.677	*	2.128E+08
6820.372	4.638	-1.120	1.40	2.218E+08
8471.739	4.956	-0.963	1.40	4.710E+08
8481.982	4.186	-1.981	1.40	6.295E+07
8514.072	2.198	-2.129	*	1.959E+07
8515.108	3.018	-1.973	1.40	7.568E+07

**Table A.1.** (continued)

Wavelength (Å)	$\chi$ (eV)	$\log gf$	$\delta\Gamma_6$	$\Gamma_{\text{rad}}$ (s <sup>-1</sup> )
Fe II				
6084.111	3.199	-3.800	2.50	3.428E+08
6113.322	3.221	-4.210	2.50	3.412E+08
6149.258	3.889	-2.870	*	3.388E+08
6432.680	2.891	-3.670	2.50	2.897E+08
6456.383	3.903	-2.250	2.50	3.373E+08
Co				
6093.143	1.740	-2.440	*	2.080E+07
6116.996	1.785	-2.590	*	2.009E+07
6454.990	3.632	-0.350	*	7.396E+07
Ni				
6108.107	1.676	-2.450	*	4.864E+07
6111.066	4.088	-0.870	*	1.455E+08
6119.749	4.266	-1.350	2.50	2.673E+08
6128.963	1.676	-3.430	*	1.211E+07
6133.963	4.088	-1.830	*	1.449E+08
6175.360	4.089	-0.559	*	2.328E+08
6176.807	4.088	-0.350	*	1.452E+08
6177.236	1.826	-3.600	2.50	4.305E+07
6183.842	4.167	-1.938	2.50	2.529E+08
6186.709	4.105	-0.960	*	2.056E+08
6482.796	1.935	-2.930	*	8.147E+07
6772.313	3.658	-0.980	*	1.500E+08

Chen Y.Q., Nissen P.E., Zhao G., Zhang H.W., Benoni T., 2000, *A&AS* 141, 491

Drake J.J., 1991, *MNRAS* 251, 369

D'Odorico S., Ghigo M., Ponz D., 1987, An atlas of the thorium-argon spectrum for the ESO Echelle Spectrograph in the  $\lambda\lambda$  3400-9000 Å region. ESO Scientific Report, European Southern Observatory (ESO), Garching

Edvardsson B., Andersen J., Gustafsson B., et al., 1993, *A&A* 275, 101

Feltzing S., 1995, Ph.D. Thesis, Astronomiska Observatoriet, Uppsala, Sweden, Acta Universitatis Upsaliensis, ISBN 91-554-3660-9 (for copies, contact the author)

Feltzing S., Gustafsson B., 1998, *A&AS* 129, 237

Feltzing S., Holmberg J., Hurley J., 2000, *A&A*, submitted

Fuhrmann K., 1998, *A&A* 338, 161

Griffin R., 1968, A photometric atlas of the spectrum of Arcturus,  $\lambda\lambda$  3600-8825 Å. Cambridge Philosophical Society, Cambridge

Gustafsson B., Bell R.A., Eriksson K., Nordlund A., 1975, *A&A* 42, 407

Gustafsson B., Kjaergaard P., Andersen S., 1974, *A&A* 34, 99

Kurucz R.L., Furenlid I., Brault J., 1984, Solar flux atlas from 296 to 1300 NM. National Solar Observatory Atlas, Sunspot, National Solar Observatory

Martin C., Mignard F., 1998, *A&A* 330, 585

Mihalas D., Binney, J., 1981, Galactic astronomy: Structure and kinematics. 2nd edition, W.H. Freeman and Co., San Francisco

Moore C.E., Minnaert M.G.J., Houtgast J., 1996, In: The solar spectrum 2935 Å to 8770 Å. National Bureau of Standards Monograph, US Government Printing Office (USGPO), Washington

Olsen E.H., 1984, *A&AS* 57, 443

Olsen E.H., 1993, *A&AS* 102, 89

Olsen E.H., 1994, *A&AS* 106, 257

O'Neill J.A., Smith G., 1980, *A&A* 81, 100

Perryman M.A.C., 1997, ESA SP-1200, 120

Piskunov N.E., Kupka F., Ryabchikova T.A., Weiss W.W., Jeffery C.S., 1995, *A&AS* 112, 525

Rentzsch-Holm I., 1996, *A&A* 312, 966

Samland M., 1998, *ApJ* 496, 155

Smith G., 1981, *A&A* 103, 351

Smith G., O'Neill J., 1975, *A&A* 38, 1

Taylor B.J., 1996, *ApJS* 102, 105

Thévenin F., Idiart T.P., 1999, *ApJ* 521, 753

Thorén P., 2000, *A&A* 358, L21

Timmes F.X., Woosley S.E., Weaver T.A., 1995, *ApJS* 98, 617